Characterization and Comparison of Galileo and GPS Anomalies

Rebecca Wang, Todd Walter

ABSTRACT

Receiver autonomous integrity monitoring (RAIM) has long relied on GPS to achieve lateral navigation by different aerospace and aviation systems. However, an advanced form of RAIM, called ARAIM, would achieve the additional function of vertical navigation. However, because vertical operations require tighter integrity capabilities than what is currently achievable by RAIM, more stringent evaluations of GNSS performance has become a greater focus, especially as new satellite service constellations such as Galileo become more operationally mature. There are two categories of satellite faults that ARAIM requires knowledge of: satellite fault, which affects each satellite independently, and constellation fault, which affects multiple satellites simultaneously due to a common cause. By analyzing GNSS performance, estimates for the likelihood of each type of fault can be obtained and its impact on ARAIM performance can be assessed. Different fault likelihoods result in different safety comparisons, thus, it is important to evaluate the fault types and their probabilities of occurrence. This paper examines the last 3 years of Galileo clock and ephemeris errors to obtain appropriate estimates for the probability of independent satellite failures, P_{sat}, and the probability of simultaneous satellite failures, P_{const}. This paper also examines the two most recent GPS faults in 2022 and 2023 and near-faults from 2017 to 2021 given that there have been no GPS faults between 2012 and early 2022, but still some anomalous events worthy of analysis.

I. INTRODUCTION

With the recent progress of the Galileo satellite constellation, a better understanding of its performance is necessary to incorporate it into various augmentation systems. These systems, including Advanced Receiver Autonomous Integrity Monitoring (ARAIM), Satellite-Based Augmentation System (SBAS), and Ground-Based Augmentation System (GBAS), all require a characterization of anomalous events and faulted behaviors for each constellation. The increase of constellations in service allow for more stringent evaluations of GNSS performance which are required for the improvement of these augmentation systems. We have adapted our tools that have been developed and extensively used to characterize GPS performance to also evaluate Galileo. Characterizing and understanding the onset of anomalous events such as sudden jumps of clock run-offs is necessary to evaluate the timely response of detection monitors. Although GPS had been fault-free since 2012, comparing and contrasting the behavior of prior fault events and recent near-fault events on GPS to recent Galileo faults can also be helpful for system design. Walter and Blanch (2015), Alonso et al. (2020), and Perea et al. (2017) are among some of past research that has been published in this area evaluating the performance of GPS and Galileo for different time periods. The rest of the introduction will introduce the contribution of our research to this field.

In 2021, two new Galileo faults were discovered with one occurring in January and the later one occurring in September. The characterization of these faults is instructive to understanding how augmentation systems designed for GPS will react to potentially different behaviors. ARAIM focuses on two types of faults: those which affect satellites independently and those which affect multiple satellites simultaneously. The likelihood of these faults in the Galileo constellation highly impact the performance of ARAIM, and the characteristics of the onset of the fault, its duration, their likelihood, etc., will be discussed. Currently, continuous, autonomous detection of anomalous events in the Galileo constellation can be processed using publicly available precise products at sampling rates up to 30 seconds. Galileo broadcast clock and ephemeris data are evaluated against the precise clock and ephemeris products provided by the International GNSS Service (IGS) network (Dow et al., 2008), and the fault rate and duration, ranging accuracy, and observed error distribution are among some of the analysis done to characterize the behavior of these faults. To this end, we draw conclusions on the performance of the current Galileo constellation by characterizing the faults detected from recent years (2018-2022).

While characterizing faults are of interest to the GNSS integrity and augmentation community and is necessary for improving augmentation systems, characterization of near-fault events is also useful for monitoring the performance of GNSS constellations. We take a look at the normalized maximum projected error (MPE) for the GPS satellite constellation over the past five years (2017-2021) and find that there are four events that exceed a normalized MPE of 2.5, two of which exceed a normalized MPE of 3. One of these events occurred in 2017, with the remaining three events occurring in 2021. The two events which exceeded a normalized MPE of 3 both occurred in 2021. Although there were no faults, the overbound for 2021 has less margin against overbounding by the instantaneous user range accuracy (IURA) than that of prior years as shown in Liu et al. (2022). These events occurred on four different satellites. In this paper, we also aim to characterize these near-fault events and understand the nature of their onset as an additional tool for satellite performance monitoring. Finally, the recent GPS faults occurring in 2022

and 2023 will be characterized and its fault probabilities will be evaluated.

II. SATELLITE ERROR SOURCES

Error sources in satellite performance can come from imperfections on the physical satellite or at the constellation ground control center, including satellite clock and ephemeris errors, ranging signal deformation errors, incoherence between the signal code and carrier, biases between signals at different frequencies, and biases in the satellite's broadcast antenna described in Hernández (2012) and Blanch et al. (2013). Ephemeris errors are caused by incorrect satellite locations transmitted by the navigation message, and it is common that the radial component error is smaller compared to the tangential and cross-track errors (Januszewski, 2017).

Other error sources exist, such as from the signal propagation environment or in the aircraft operation environment, but these sources are not controlled by the satellite performance. These error sources include ionospheric error, tropospheric error, multipath, receiver antenna group delay, noise and interference, and receiver antenna biases. In these cases, several methods exist to mitigate these error sources. For example, the ionospheric error can be corrected through applying a model of the ionosphere with several (eight) coefficients broadcast in the navigation message in the case of a single frequency receiver; in the case of dual frequency receivers, the simultaneous measurement of the pseudorange from both satellite frequencies can reduce the error. These satellite error sources induce nominal ranging errors, meaning that there is always some amount of error corrupting the true position solution. The user range accuracy parameter, σ_{URA} bounds this nominal error. Furthermore, besides the nominal error, there is also a probability associated with the errors that exceed a defined threshold made by the service provider which are called faults. Though rare, there are two categories of faults. Faults affecting only one satellite over a particular time duration is referred to as"narrow" and faults affecting more than one satellite over a particular time duration is referred to as "wide". The probability of a narrow fault, P_{sat}, and the probability of a wide fault, P_{const}, along with the σ_{URA} are used in the airborne algorithm.

III. PERFORMANCE EVALUATION PROCEDURE

Because the largest errors in the list of common satellite error sources are the clock and ephemeris errors, they are characterized for Galileo in this paper using data from the IGS network. The navigation data files undergo a voting process specified in Gunning et al. (2017) which screens for outliers and cleans up the recorded broadcast navigation messages into one set of navigation messages for a chosen constellation per day. Which broadcast message to keep in the final set for each epoch is done through specific validity interval checks against the broadcast SISA/URA/health values as well as through a majority vote. These are used to evaluate the satellite position and clock real-time broadcast estimates. Then, at each epoch, a comparison is able to be made between the cleaned set of broadcast navigation data and the precise navigation data.

IV. GALILEO SERVICE HISTORY

Figure 1 shows an overview of the Galileo data analyzed. On the vertical axis is the satellite labeled by their service vehicle number (SVN). Each color or symbol on each horizontal line indicates a satellite status or measurement type for each satellite. The green color indicates a broadcast ephemeris that was set healthy and that there was a valid comparison made to the precise ephemeris provided. The blue color indicates that the broadcast ephemeris was unhealthy and thus there was no valid comparison. The magenta color indicates that there was no broadcast ephemeris provided by IGS but that there were still precise ephemeris estimates available. The yellow color indicates that there were still broadcast ephemeris available but no precise ephemeris estimates found. The black color indicates that the satellite was operational but that there were no recorded broadcast nor precise ephemeris estimates available. Finally, the gray line in the background indicates that the satellite was not operational. In the case of the Galileo constellation, because of its recent development, this could be due to the fact that the satellite was not yet launched or broadcasting, although a decommissioned satellite would also be indicated by this line. We can see that there are no yellow or black points in Figure 1 since when these do occur, a manual attempt is made to fill in the missing data as best as possible.

1. Galileo Fault Definition

According to the Galileo Open Service Service Definition Document (OS SDD) (noa, 2021), a Galileo satellite is considered to be faulted if the average projected error is greater than 4.17 x σ_{URA}, where σ_{URA} is defined to be a constant 6 m value. In the future, this value will be broadcast. As can be seen in Figure 1, there are four faults that occurred, accumulating a total of 1.6 satellite hours in a faulted state over a four and a half year period. The events are listed below:

PRN	SVN	Date	UTC Time
11	101	October 29, 2019	18:05 – 18:45
12	102	January 21, 2021	01:39 – 02:01
1	210	September 5, 2021	05:43 – 6:02
1	210	April 29, 2022	01:00 – 01:12

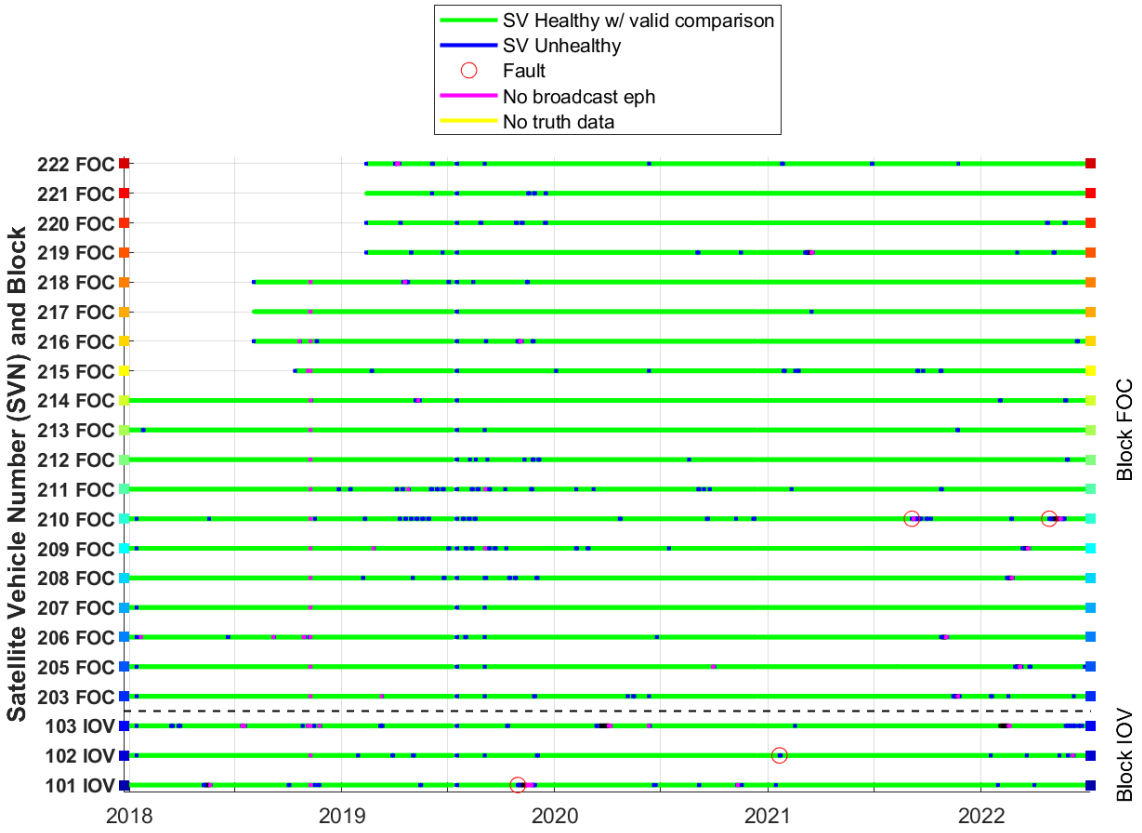

Figure 1: Summary of observations for each satellite from 2018 to end of June 2022. Green indicates satellites with valid observations, blue indicates satellites which are unhealthy, pink indicates instances where there is no broadcast ephemeris, and red circles indicate a fault. The faint gray line indicates that the satellite was not yet in operation.

These events have been further studied by utilizing thirty-second precise clock data made available by the center for orbit determination in Europe (CODE) (Peter et al., 2009) in combination with the fifteen-minute IGS precise ephemeris and clock data.

2. Galileo Detailed Fault Event Analysis

Figure 2 shows the October 29, 2019 event which affected PRN 11. As shown in the second sub-graph, at 17:55 the clock began to ramp in an unbounded manner. During this event, the broadcast signal-in-space-accuracy (SISA) was at 3.12 m until the SISA is set to the state of no-accuracy-prediction-available (NAPA). At roughly 18:05, the error exceeded the fault definition and roughly 40 minutes later, at 18:45, it was set to the NAPA. The clock error grows to be 500 m at the end of its fault duration, after which it grows to be greater than 5000 m during its marginal/unhealthy status. As can be seen in the first sub-graph, the ephemeris data was not affected by the clock error. The marginal/unhealthy status persists for greater than one day, where the radial, along-track, and cross-track errors then follow suit and become inflated as well. The total faulted time duration is 40 minutes. Almost one month later, on November 28, 2019, the satellite was set to healthy.

Galileo satellites have several methods slightly different to GPS satellites to indicate an unhealthy satellite. Primarily, the

Signal-In-Space (SIS) Status can assume one of three values: healthy, unhealthy, and marginal (noa, a). The SIS status is broadcast within the navigation message through three SIS Status Flags. They are the Signal Health Status (SHS) flag, the Data Validity Status (DVS) flag, and the Signal-In-Space Accuracy (SISA) value. The SHS flag can take on four different states, the DVS flag can take on two states, and the SISA value can take on two states; different combinations of the SHS, DVS, and SISA states indicate the final SIS Status which can be found in noa (a). In each of the Galileo faults examined below, the unhealthy status traditionally referred to for unhealthy GPS satellite status is first indicated by the marginal status in Galileo satellites, in particular through setting the SISA value to the index indicating No Accuracy Prediction Available (NAPA).

Figure 3 shows the January 21, 2021 event affecting PRN 12. However, the higher-sampling rate of 30-seconds is missing after completing the data processing at the start of the fault period. Further data processing is necessary to determine whether the event was caused by a clock jump or clock ramp, but the fault is still caused by a clock error. The MPE for this fault is the smallest compared with the MPEs of the other three Galileo faults at around 30 m. The total faulted time duration is estimated to be 22 minutes. Sometime between 01:37 and 01:39, the satellite enters into the faulted state, until 22 minutes later, at roughly 02:01, the satellite enters into the marginal/unhealthy state.

Figure 4 shows the September 5, 2021 event affecting PRN 1. This event is another clock ramp that is similar to the October 29, 2019 fault event. The ramp starts around 05:41 and exceeds 4.17 x σ_{URA} at about 05:43, with a final fault duration period of about 19 minutes. At 06:02, the satellite enters into the marginal/unhealthy state. The error grows to be around slightly over 500 m during the faulted period, and greater than 5000 m during the marginal/unhealthy period. The unhealthy state of this satellite persists for weeks before a correction is made at September 21, 2021 when the satellite is healthy again.

Finally, Figure 5 shows the April 29, 2022 event affecting PRN 1. This fault is also a clock ramp, similar to the 2019 and latter 2021 fault. The ramp starts around 00:58 and exceeds the threshold at around 01:00. This fault also has a relatively low settling MPE of about 250 m. The October 29, 2019 and September 5, 2021 faults all have MPEs that reach the thousands or greater and require a much longer time to settle before receiving correction. The fault duration lasts about 12 minutes, in which the -1 SISA value is broadcast at 01:12. After almost one month, on May 25, 2022, the satellite is set to healthy again.

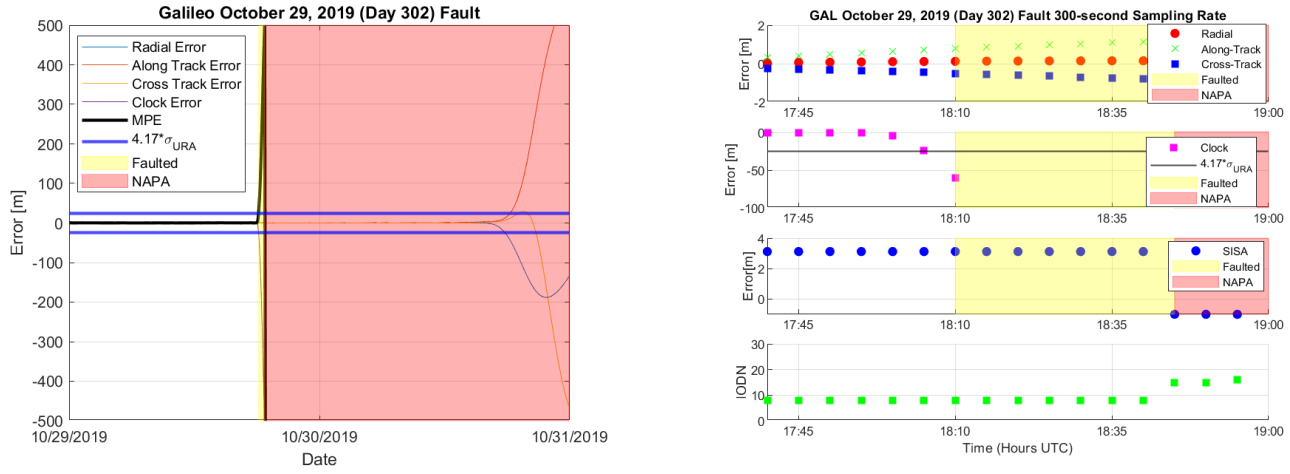

(a) Overview

(b) Zoomed-in

Figure 2: Fault event for PRN 11 on October 29, 2019.

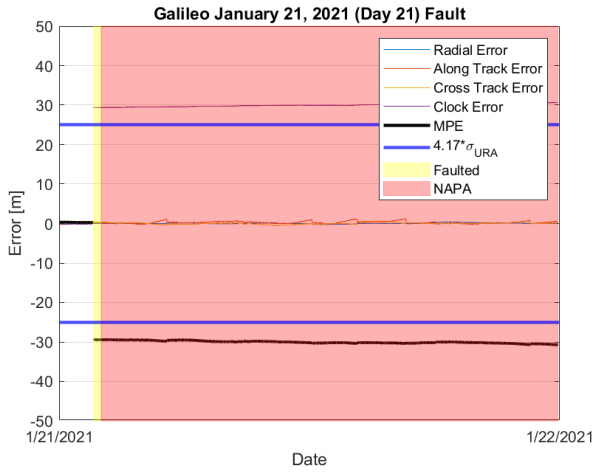

(a) Overview

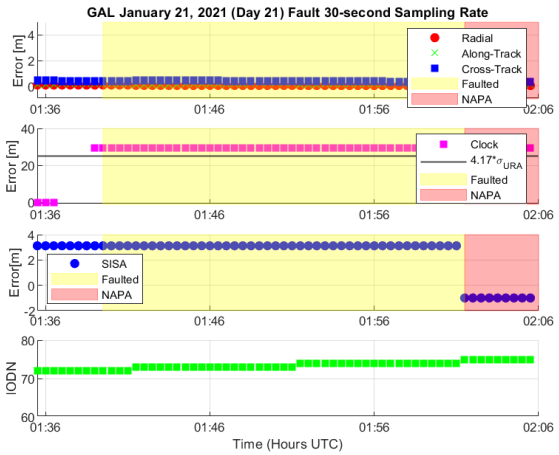

(b) Zoomed-in

Figure 3: Fault event for PRN 12 on January 21, 2021.

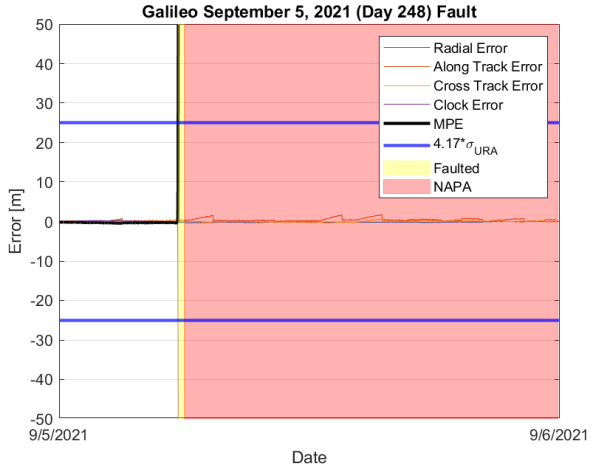

(a) Overview

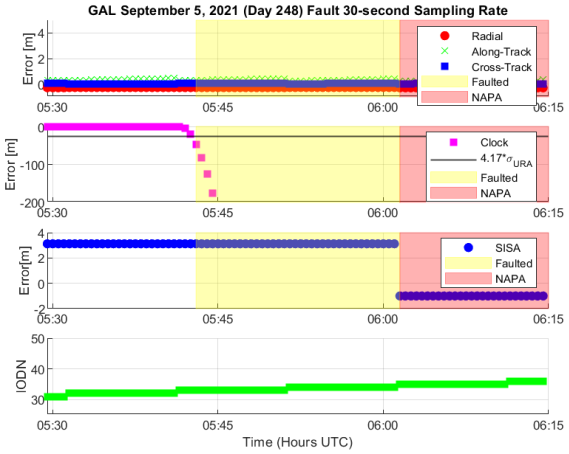

(b) Zoomed-in

Figure 4: Fault event for PRN 1 on September 5, 2021.

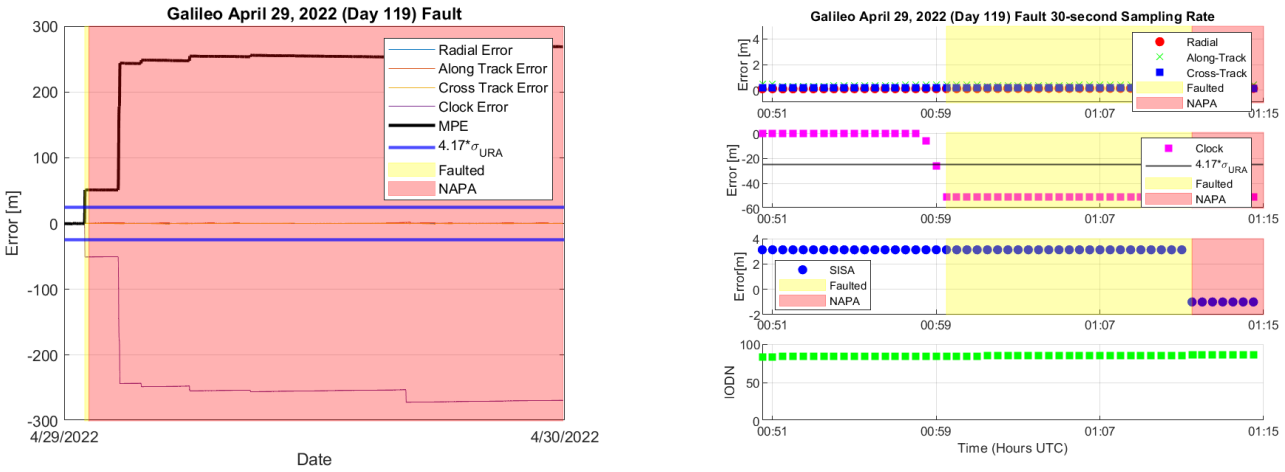

(a) Overview

(b) Zoomed-in

Figure 5: Fault event for PRN 1 on April 29, 2022.

V. OBSERVED GALILEO FAULT PROBABILITIES

This section aims to describe the observed Galileo fault probabilities based on the faults observed in the satellite constellation operation time. ARAIM airborne algorithms examines subset solution comparisons in order to confirm inconsistencies (Blanch et al., 2012). Then, the airborne algorithm is able to maintain integrity as expected if the true probability of encountering such failures is below the assumed probability. The Galileo OS SDD states that the probability that any satellite of the Galileo operational satellite service provides an instantaneous SIS range error which is greater than k times the Galileo URA and under the condition that no notification is given to the user i.e. the satellite is not indicated as unhealthy is defined as the probability of a satellite fault, P_{sat} noa (2021). The factor k is chosen to be the number of standard deviations from the mean corresponding to a probability of P_{sat} in a normal distribution, where P_{sat} is defined as less than or equal to 3x10^{-5}. In this case, k is 4.17 for $P_{sat} \leq$ 3x10^{-5}.

To calculate the narrow and wide fault probabilities, we use the following method from Walter et al. (2019):

$$R = \frac{k + 0.5}{T} \tag{1}$$

$$P_{sat} = R * MTTN \tag{2}$$

where k is the number of events observed, T is the time interval of observed events, and $MTTN$ is the mean time to notify the user. We assume an $MTTN$ of 1 hour, although this is not set by Galileo but rather chosen arbitrarily and conservatively, given the largest MTTN from the previous observed faults is 40 minutes. The narrow or wide fault probabilities can then be obtained by using the corresponding total time duration of observed events.

Figure 1 shows the history of Galileo satellite observation from January 2018 through June 2022. During this time, there have been four faults observed with a total duration of roughly 93 minutes, an average faulted time duration of 23 minutes. Taking into consideration the different times when satellite vehicle 215 though 222 went into operation, the collected data totaled more than 797,160 valid satellite hours, but we used 797,160 hours for the total fault duration for easier calculation (by counting satellites 215 through 222 to have a three and a half year operating time over the four and half year period analyzed). This duration is made up of the time when the satellites broadcasted valid signals and were in the healthy status. Using Equations 1 and 2, the observed data implies an average onset fault rate of 5.6 x 10^{-6} and a P_{sat} of 2.2 x 10^{-6}. Therefore, based on these numbers, there is more than a factor of 13 between the observed fault probability and the extreme upper bound of the fault probability from the Galileo OS SDD. Some degree of conservatism is expected, as the numbers in the Galileo OS SDD are meant to represent upper bounds and not the actual values.

Beyond narrow faults, there is a consideration that needs to be made for the possibility of wide faults also known as constellation faults, or P_{const}. This is when the fault can lead to abnormally large errors on more than one satellite at a time due to a common cause. The Galileo OS SDD does not discount the reality that many faults can occur at the same time, and the maximum

expected value of the Galileo probability of constellation fault is 2x10^{-4}. To calculate P_{const}, we use the same fault probability calculation methodology as above but with a T equaling the number of constellation hours, which in this case is roughly 39,420 hours. Because we did not observe any wide faults in the history of Galileo data analyzed, we use $k = 0$, and we obtain a P_{const} of 1.3 x 10^{-5}.

VI. OBSERVED ERROR DISTRIBUTION

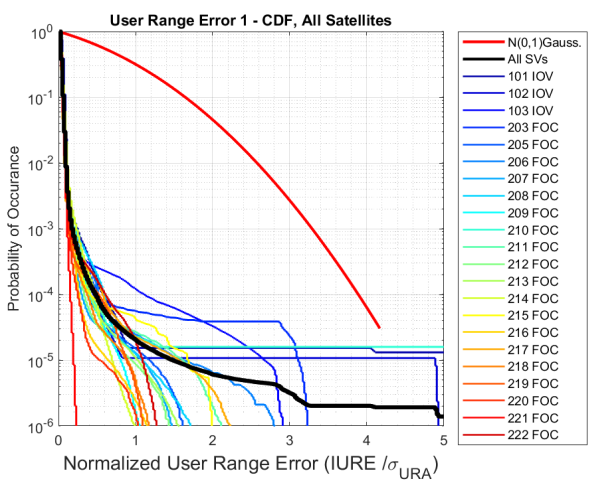

(a) CDF of normalized maximum projected ranging errors for all satellites.

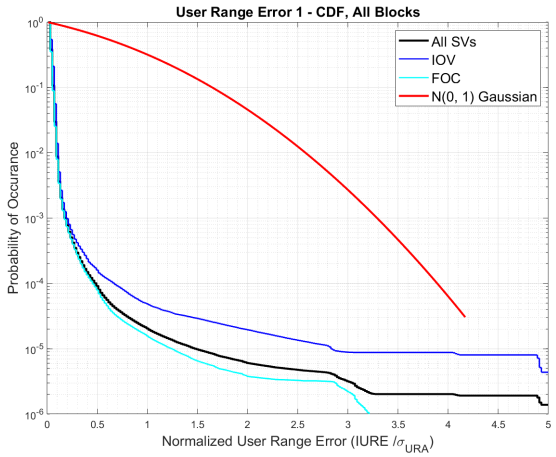

(b) CDF of normalized maximum projected ranging errors grouped by satellite block.

Figure 6: Error distributions for Galileo performance history.

The observed failures can be used to calculate a historical fault rate. Walter and Blanch (2015) found that between 2008-2015, the characterization of GPS performance errors showed that errors are typically much lower than the fault threshold, and when they exceed the fault threshold, the errors are generally much, much larger. We find this trend to be even more exaggerated from the Galileo service constellation.

Figure 6a shows one minus the cumulative distribution function (CDF) for the MPE for each satellite, and Figure 6b shows one minus the CDFs but grouped by Galileo satellite block type. At the time of writing, the Galileo satellites are divided into two block types: in-orbit validation (IOV), and full operational capability (FOC). The thick black line indicates the aggregate CDF of all satellites, and the thick red line is the expected CDF value which corresponds to a normal distribution with zero-mean and unity variance. The red line extends down to the 3 x 10^{-5} probability level because that is the guarantee provided by the Galileo OS SDD. Beyond this line, nominal Gaussian behavior is not guaranteed.

We can see that despite the errors accumulated from the fault events, the three observed faults do not exceed the thick red line (SVNs 101, 102, 210).

Figure 6b shows the distribution over the time period analyzed for Galileo satellite blocks. There is value in combining the data together by satellite blocks because there may be correlation in behavior between satellites of the same block due to the similarity, if not identical, design amongst satellites of the same block.

We can see that the FOC satellites have the smallest errors and fault likelihood, even though the previous satellite faults spanned both satellite blocks. Despite the difference in performance, the broadcast σ_{URA} describes the nominal clock and ephemeris extremely conservatively as can be seen from the wide margin between the error curve of the satellite blocks and the bounding Gaussian distribution line. This large margin indicates that it would be worthwhile to investigate a minimum scale factor which causes the broadcast σ_{URA} to just touch the bounding red line when multiplied by it, which can be used to guide future messages from Galileo to broadcast smaller σ_{URA} values.

VII. GPS SERVICE HISTORY

The clock and ephemeris errors were characterized for GPS in a nearly identical manner to those of the Galileo constellation satellites with a few exceptions. The precise estimates were provided by the National Geospatial Intelligence Agency (noa, c) due to easier data processing given the provision of data with the antenna phase center location.

1. GPS Fault Definition

According to the GPS standard positioning service performance standard (GPS SPS PS) (noa, b), a satellite is considered to be faulted if the average projected error is greater than 4.42 x σ_{URA}. Same as the Galileo data analysis, we preserve our stricter criteria that the satellite is deemed as faulted if the project error at any point on the earth is greater than 4.42 x σ_{URA}. A significant difference to the Galileo operation is that the σ_{URA} for GPS is dynamic and broadcast most often as 2.4 meters, although 3.2 meters will also be broadcast occassionally. Evaluating near-fault events to be errors that are $\geq$ 2.5 x σ_{URA}, it can be seen in Figure 7 that there are four near-fault events that occurred. The events are listed below:

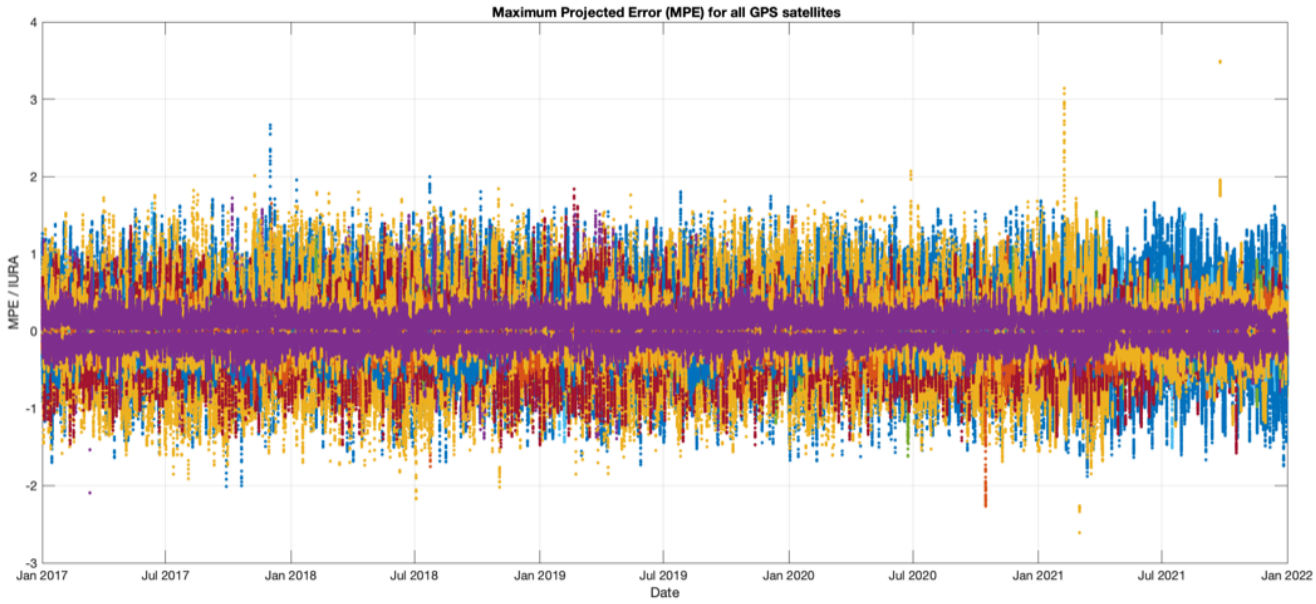

Figure 7: Overview of the normalized MPE of all GPS satellites from January 2017 to January 2022.

PRN	SVN	Date	UTC Time
22	47	December 1, 2017	(Nov. 30) 19:50 – (Dec. 1) 10:40
17	53	February 7, 2021	17:00 – 21:15
3	69	March 2, 2021	07:10 – 08:15
10	73	September 24, 2021	11:55 – 14:15

Although an analysis of the GPS P_{sat} and P_{const} values may not be necessary based on these near-fault events, it is useful to examine the behavior of these higher-than-normal MPE values.

Finally, the two most recent GPS faults occurring in 2022 and 2023 are listed below and discussed in detail in later sections.

PRN	SVN	Date	UTC Time
12	58	October 2, 2022	15:10 – 15:55
1	63	January 25, 2023	16:10 – 17:15

2. GPS Near Fault Events

Figure 8 describes a near-fault event that occurred at the end of the day on November 30, 2017 and lasted into December 1, 2017. The near-fault was lead by an along-track error that ramped slowly starting around 19:50, with the cross-track error ramping slowly shortly after, around 21:40. These two components maintained an overall increasing trend until around December 1, 2017 at 10:40. During this entire time, the clock error remained normal, and it seems that a new issue of data: clock (IODC) to broadcast a new ephemeris was broadcast around 10:05, and only lasted roughly 40 minutes before a new IODC upload around 10:40 that corrected the error.

Figure 9 shows the second near-fault event on February 7, 2021 affecting PRN 17. Here we see that the abnormal event is caused by a clock ramp that begins around 17:00 and lasts about four hours until the clock ramp seems to be corrected by a new IODC broadcasting new ephemeris set.

Figure 10 shows the March 2, 2021 near-fault event affecting PRN 3 at 07:10. This event is caused again by a clock error. Although the error seems to be from a clock jump, higher-sampling-rate data processing can be performed on this example to confirm whether the error is caused by a clock jump or clock ramp. The event lasts for about one hour until a new IODC is broadcast around 08:25 which seems to correct the abnormal clock error.

Finally, Figure 11 shows the September 24, 2021 near-fault event affecting PRN 10. The event seems to be caused by a clock jump error around 11:55 but can benefit from higher-sampling-rate data processing to examine whether there was a ramp at the onset of the near-fault event. The clock data then seems to undergo a series of jumps at above normal error values following the new sets of ephemeris broadcast by new IODCs that align with the start and end of the clock jumps. Finally, after about 2.25 hours of anomalous behavior, the clock error returns back to normal levels around 14:15.

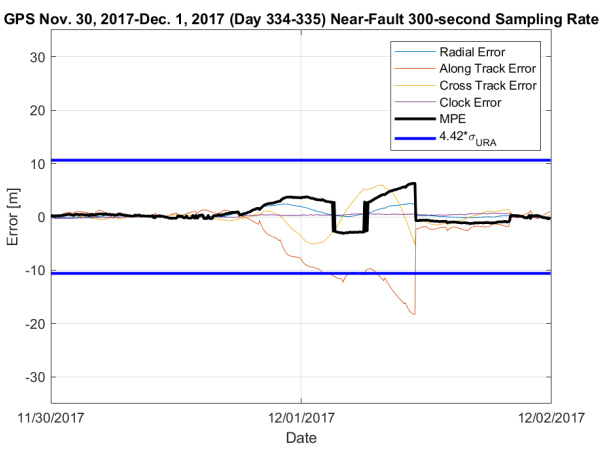

(a) Overview

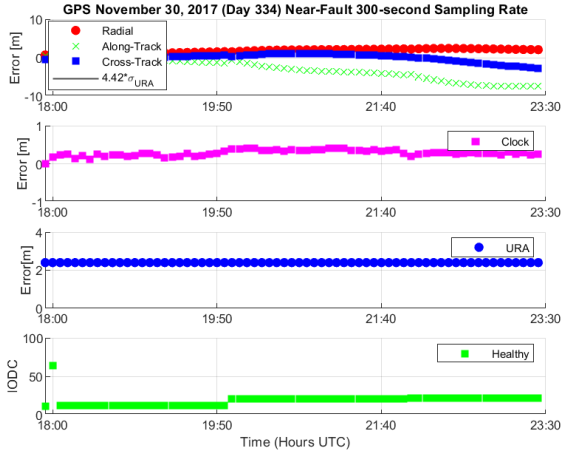

(b) Day 334 Zoomed-in

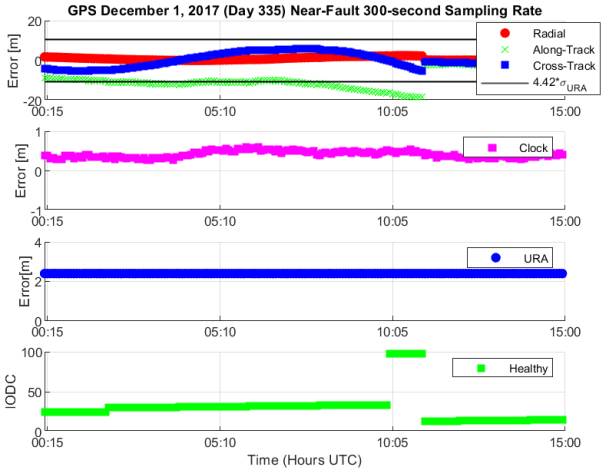

(c) Day 335 Zoomed-in

Figure 8: Near-fault event for PRN 22 on November 30, 2017 - December 1, 2017.

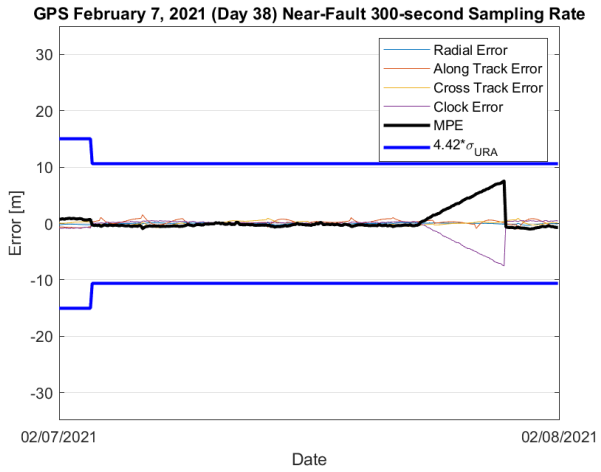

(a) Overview

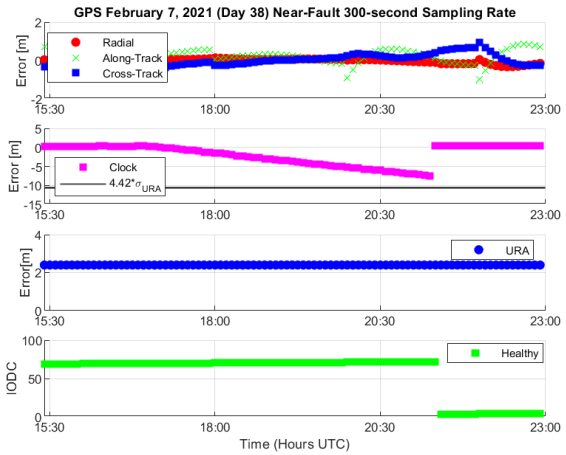

(b) Zoomed-in

Figure 9: Near-fault event for PRN 17 on February 7, 2021.

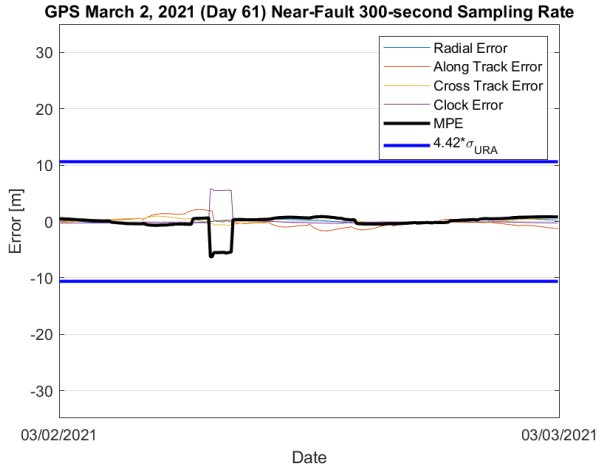

(a) Overview

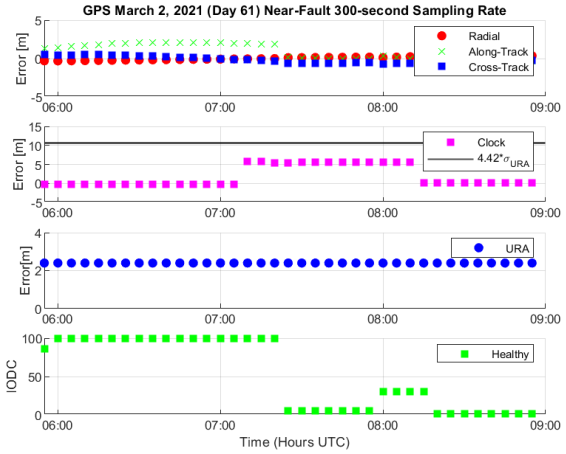

(b) Zoomed-in

Figure 10: Near-fault event for PRN 3 on March 2, 2021.

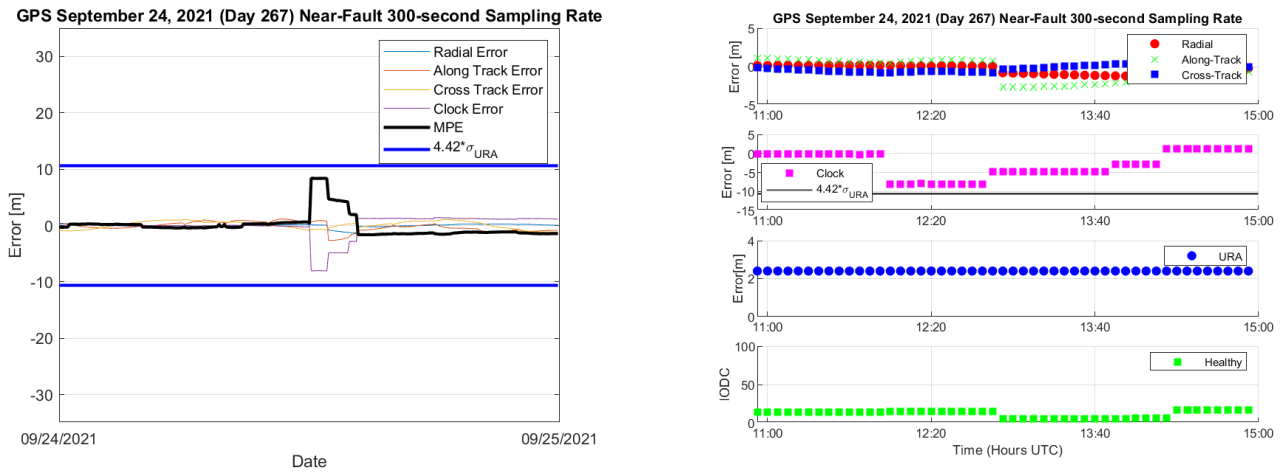

(a) Overview

(b) Zoomed-in

Figure 11: Near-fault event for PRN 10 on September 24, 2021.

3. GPS Detailed Fault Analysis

There had been no observed GPS faults for a period of more than ten years since June 17, 2012 until October 2, 2022 (Walter and Blanch, 2015). Figure 12 shows the October 2, 2022 fault occurring on PRN 12 (SVN 58). Here, the broadcast σ_{URA} is demonstrated more obviously by the bump in the blue line representing the fault definition, where the small bump is when the navigation message broadcast a σ_{URA} of 3.2 meters instead of 2.4 meters. The fault was led by a slow clock ramp that starts around 10:20 and ramps for about five hours before finally crossing the fault definition at around 15:10. After this time, the satellite is in a faulted state for about 45 minutes before the satellite corrects itself through a new IODC upload. Interesting to note is that the satellite never enters into an unhealthy status, and instead self-corrects during the faulted period when a new IODC is uploaded. This behavior is not typical, but was demonstrated in the two previous faults on April 25, 2010 and June 17, 2012 shown in the analysis done by Walter and Blanch (2015).

A second recent fault occurred on January 25, 2023 on PRN 1 (SVN 63). Here, the fault is caused by a clock error and seems to occur at the onset of a clock jump occurring at roughly 16:10. The faulted duration lasts for about 185 minutes until roughly 19:15, when the satellite is set unhealthy due to a new IODC. The maximum clock error of about 27 meters is large enough to significantly exceed the fault definition. This fault duration is significantly larger than any of the previous fault durations since 2008. At approximately 15:45 on January 26, 2023, the satellite returned to a healthy state.

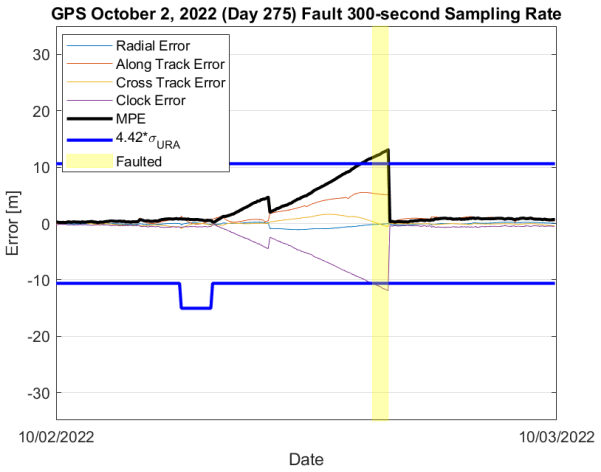

(a) Overview

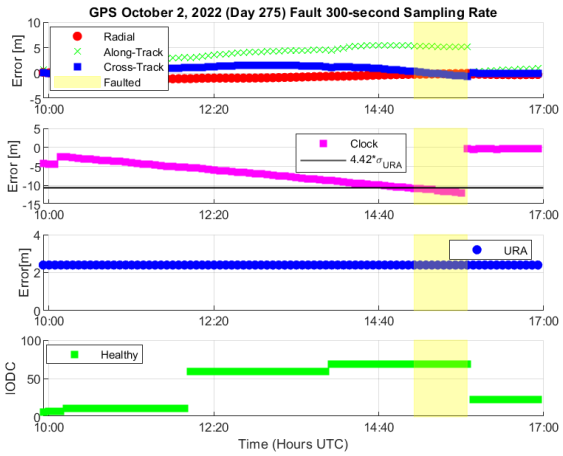

(b) Day 275 zoomed-in.

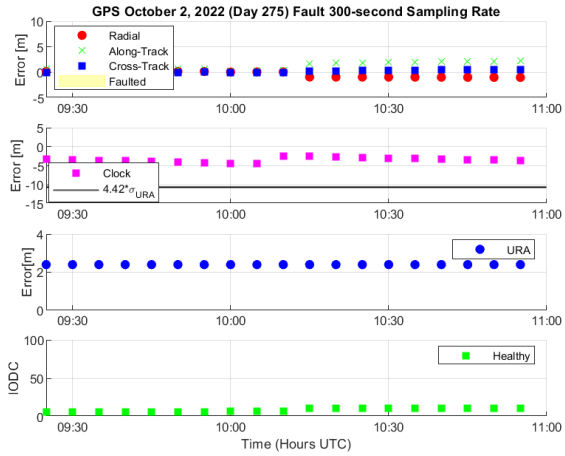

(c) Day 275 zoomed into beginning clock ramp period.

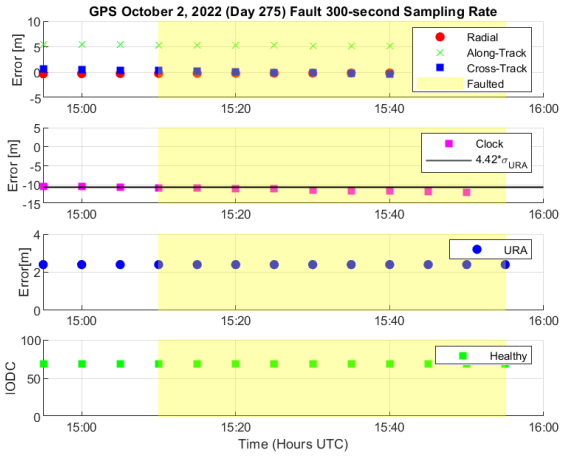

(d) Day 275 zoomed into fault period.

Figure 12: Fault event for PRN 22 on November 30, 2017 - December 1, 2017.

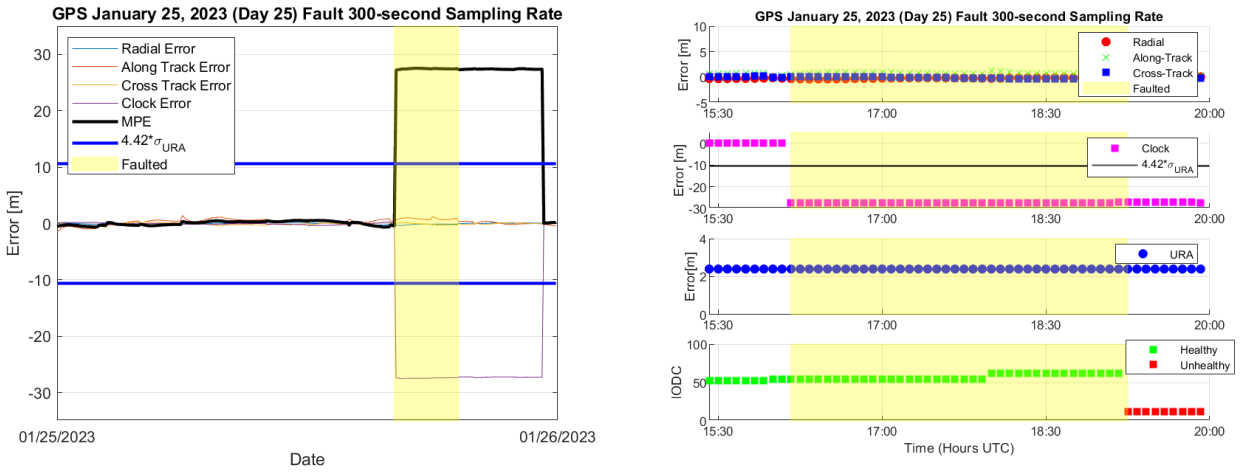

(a) Overview

(b) Day 25 zoomed into fault period.

Figure 13: Fault event for PRN 1 on January 25, 2023.

VIII. OBSERVED GPS FAULT PROBABILITIES

Walter and Blanch (2015) used an estimated 1.75 hours of cumulative faulted duration in the previous five GPS faults that occurred between 2008 to 2012. Using the same method as with the Galileo fault probability calculation with an additional 45 minutes of faulted duration from the 2022 fault and an additional 185 minutes of faulted duration from the 2023 fault, we obtain a total 335 minutes of faulted duration over a period of fifteen years, from January 2008 to January 2023. This gives an average faulted time duration of approximately 48 minutes and a total estimated valid satellite hours of 3,967,200 hours. Using the same method to calculate the probability of satellite fault, with $k = 7$ due to 7 total observed faults, this therefore gives an average onset fault rate of 1.9 x 10^{-6} and a GPS probability of satellite fault, $P_{sat} \approx 1.5$ x 10^{-6}. Given the GPS service provider P_{sat} commitment of 1 x 10^{-5}, this value is more than 6 times smaller than the specified P_{sat}.

Similar to before, a new probability of a wide fault can be calculated. We choose to use the same MTTN of 1 hour which is conservative, with $k = 0$ as there have been no wide faults observed, and a total time interval of observed events to be a little more than fifteen years, from January 2008 to January 2023, which results in about 132,240 hours. This gives an observed GPS probability of constellation fault, $P_{const} \leq 3.8$ x 10^{-6}.

IX. CONCLUSIONS

We have analyzed the past four and a half years of Galileo data in order to characterize the probabilities that one or more satellite is likely to be in a faulted state. We have found that for a total of four faults over four and a half years, the cumulative fault duration of approximately 97 minutes corresponds to an observed narrow probability of fault of 2.2 x 10^{-6}, which is much lower than the commitment made by the Galileo service providers. In this time period of data analyzed, there have not been any observed instances of simultaneous faults on several satellites, and we find a P_{const} less than or equal to 1.3 x 10^{-5} using a total of 4.5 years of operating duration. These values indicate that the Galileo service commitment values are conservative by a factor of 13 and 15 for the narrow and wide fault probabilities, respectively. For the GPS constellation, the addition of the sixth and seventh fault analyzed since 2018 resulted in an observed P_{sat} of 7.1 x $10^{-}7$ and a P_{const} less than or equal to 3.8 x 10^{6}; the seventh fault analyzed resulted in an observed P_{sat} of 1.5 x $10^{-}6$ and a P_{const} less than or equal to 3.8 x 10^{6}. This shows that the GPS commitment for the probability of satellite fault is conservative by over a factor of 6 for the evaluated service duration. Additionally, we have examined the anomalous events from the GPS operating history from the past five and a half years, discovering that the majority of large MPE values arose from clock errors and could last anywhere from one hour to thirteen hours before a correction is made. There were more near-fault events occurring in the GPS constellation than in the Galileo constellation, and in general, the Galileo constellation takes a much longer time to return a satellite to a healthy state whereas the GPS constellation was much quicker to provide corrections and return the satellite to healthy state. In the future, it is worthwhile to examine the near-fault events from GPS data at higher sampling rates and to characterize the nominal accuracy of the Galileo and GPS constellation performance as well as completing further analysis on the Galileo overbounding parameter for the σ_{URA} value, such as in the work done in Liu et al. (2023).

ACKNOWLEDGEMENTS

We gratefully acknowledge the support of the FAA Satellite Navigation Team for funding this work under Memorandum of Agreement : 693KA8-22-N-00015.

REFERENCES

European GNSS (Galileo) Open Service Signal-In-Space Operational Status Definition.

Global Positioning System Standard Position Service Performance Standard, 5th Edition, September 2020.

NGA Geomatics - GNSS.

(2021). EUROPEAN GNSS (GALILEO) OPEN SERVICE - SERVICE DEFINITION DOCUMENT. (1):70.

Alonso, M. T., Sanz, J., Juan, J. M., Rovira García, A., and Casado, G. G. (2020). Galileo Broadcast Ephemeris and Clock Errors Analysis: 1 January 2017 to 31 July 2020. *Sensors*, 20(23):6832.

Blanch, J., Walter, T., Enge, P., Lee, Y., Pervan, B., Rippl, M., and Spletter, A. (2012). Advanced RAIM User Algorithm Description: Integrity Support Message Processing, Fault Detection, Exclusion, and Protection Level Calculation. page 23.

Blanch, J., Walter, T., Enge, P., Wallner, S., Fernandez, F., Dellago, R., Ioannides, R., Fernandez-Hernandez, I., Belabbas, B., Spletter, A., and Rippl, M. (2013). Critical Elements for a Multi-Constellation Advanced RAIM. *Navigation*, 60.

Dow, J., Neilan, R., and Rizos, C. (2008). The International GNSS Service in a Changing Landscape of Global Navigation Satellite Systems. *Journal of Geodesy*, 83:191–198.

Gunning, K., Walter, T., and Enge, P. (2017). Multi-GNSS Constellation Anomaly Detection and Performance Monitoring. pages 1051–1062. ISSN: 2331-5954.

Hernández, I. F. (2012). EU-US Cooperation on Satellite Navigation. page 76.

Januszewski, J. (2017). Sources of Error in Satellite Navigation Positioning. *TransNav, International Journal on Marine Navigation and Safety od Sea Transportation*, 11(3).

Liu, X., Wang, R., Blanch, J., and Walter, T. (2022). Evaluation of Satellite Clock and Ephemeris Error Bounding Predictability for Integrity Applications. pages 34–43, Denver, Colorado.

Liu, X., Wang, R., Blanch, J., and Walter, T. (2023). Satellite Clock and Ephemeris Error Bounding Characterization for Galileo and GPS. Long Beach, California, ION ITM 2023.

Perea, S., Meurer, M., Rippl, M., Belabbas, B., and Joerger, M. (2017). URA/SISA Analysis for GPS and Galileo to Support ARAIM. *NAVIGATION*, 64(2):237–254. _eprint: https://onlinelibrary.wiley.com/doi/pdf/10.1002/navi.199.

Peter, H., Dach, R., Jäggi, A., and Beutler, G. (2009). High-rate GPS clock corrections from CODE: Support of 1 Hz applications. *Journal of Geodesy*, 83:1083–1094.

Walter, T. and Blanch, J. (2015). KEYNOTE - Characterization of GNSS Clock and Ephemeris Errors to Support ARAIM. pages 920–931. ISSN: 2331-6284.

Walter, T., Blanch, J., Gunning, K., Joerger, M., and Pervan, B. (2019). Determination of Fault Probabilities for ARAIM. *IEEE Transactions on Aerospace and Electronic Systems*, 55(6):3505–3516. Conference Name: IEEE Transactions on Aerospace and Electronic Systems.